Korean J. Chem. Eng., 33(4), 1211-1219 (2016)
DOI: 10.1007/s11814-015-0263-z

pISSN: 0256-1115
eISSN: 1975-7220

A pore-scale model for microfibrous ammonia cracking microreactors via lattice Boltzmann method

Gholam Reza Molaeimanesh† and Mohammad Hosein Sanati Davarani

Research Laboratory of Automotive Fluids and Structures Analysis, Automotive Engineering School, Iran University of Science and Technology, Tehran 16846-13144, Iran
(*Received 7 September 2015 • accepted 26 November 2015*)

Abstract−Microfibrous microreactors with high reactive surface-to-volume ratio are good choices for ammonia cracking, which is one of the main strategies for CO-free hydrogen production. In the current study, a numerical model based on the lattice Boltzmann method (LBM) is presented to investigate ammonia cracking microreactors with coupled physiochemical thermal processes at the pore scale. Several sets of transport phenomena such as fluid flow, species transport, heat transfer and chemical reaction are taken into account. Moreover, to model the species transport in the ammonia cracking microreactor an active approach is applied for the first time. The model is validated and then employed to simulate the reactive transport in five different microreactors with dissimilar structural parameters. Comparison of the results shows that the fibers orientation is an effective geometric parameter that can greatly influence the hydrogen production efficiency.

Keywords: Ammonia Cracking Microreactor, Lattice Boltzmann Method, Pore-scale Model, Microfibrous Microreactor, Post Microreactor

INTRODUCTION

Hybrid electric vehicles (HEVs) and fuel cell vehicles (FCVs), which are compatible with sustainable development, are currently the leading solutions for the energy and pollution crisis [1]. Decomposition of ammonia as an abundant, hydrogen-containing compound is the simplest process to achieve CO free hydrogen for fuel cell applications [2,3]. Microreactors with characteristic lengths in the micrometer range propose high surface-to-volume ratio, which leads to higher heat and mass transfer rates [4-7]. They can be attractive choices in fast catalytic reactions such as ammonia cracking [8]. Several types of ammonia cracking microreactors such as micro channel microreactors, packed-bed microreactors, post microreactors and microfibrous microreactors have been investigated experimentally and numerically [9].

In the current study, a novel pore-scale lattice Boltzmann model for simulation of reactive endothermic ammonia flow through microreactors is presented. To demonstrate the capabilities of the presented model, the effects of some geometrical parameters of ammonia cracking microreactors are investigated by simulating five different microreactors with dissimilar microstructures. The concluding remarks will be helpful to achieve more efficient structural design of microreactors. Three of the investigated microreactors are microfibrous ones. To the best of the authors' knowledge, ammonia cracking microfibrous microreactors have not been simulated at pore scale up till now.

Considering the anisotropic and non-homogeneous microstructure of microfibrous microreactors, the use of a pore-scale simulation technique will lead to more realistic results. However, since conventional macro scale methods need less computational effort, they are still adopted for microreactor simulations. Recently, some interesting investigations based on these methods have been performed [10-12].

Lattice Boltzmann method (LBM) is a suitable numerical technique for pore-scale simulation of complex fluid systems. It offers interesting features, such as ease of dealing with complex boundaries, parallelization of the algorithm and modeling multiphase fluid flow in anisotropic and non-homogeneous porous media [13].

Recently, some LB simulations of microreactors with different flow field configurations have been performed. Most of the simulated microreactors are packed-bed ones [14-20], which are not a promising type due to their low heat and mass transfer efficiency. Moreover, the chemical reactions considered in such investigations are temperature independent, so there is no need to model the temperature field in the microreactor. However, the ammonia decomposition reaction is strongly temperature dependent. Hence, to simulate an ammonia cracking microreactor, the temperature field must be modeled while coupled with reactive ammonia flow.

To the best of the authors' knowledge, only Chen et al. [21] performed an interesting LB simulation of a post microreactor considering coupled physiochemical thermal processes of ammonia decomposition. They assessed the effects of ammonia flow rate, operating temperature and some geometrical parameters [21]. They modeled multi-species flow through a passive approach, i.e., they considered ammonia as the dominant species (solvent), and the velocity field has been solved only for ammonia. Afterward, the concentration of hydrogen and nitrogen species was determined by solving the concentration field. This approach may lead to a

†To whom correspondence should be addressed.
E-mail: molaeimanesh@iust.ac.ir

lack of accuracy, especially when species fractions are comparable and no species can be considered as the solvent [22]. Such condition may happen frequently in microreactors with fast reaction rates, such as ammonia cracking microreactors. Since the concentration of ammonia (solvent) in some regions of the microreactor can approach zero, we consider coupled physiochemical thermal processes through an active approach for the first time. In an active approach, the velocity fields of all species are solved.

In the present study, three microfibrous microreactors and two post microreactors with different structural parameters, but the same catalyst mass, are simulated by LBM to have a better understanding of the role of some geometrical parameters on the performance of an ammonia cracking microreactor. The numerical model applied for these 2D simulations can be applied for further 3D simulating of a microfibrous microreactor with a realistic representation of the porous medium via SEM/TEM techniques and computer clusters.

NUMERICAL METHOD

1. LBM Framework

Lattice Boltzmann method is a powerful numerical modeling technique. In this method, a fluid is assumed to be composed of virtual fluid particles that move and collide with each other in a lattice structure. These particles are treated by a distribution function rather than by positions and velocity vectors [23]. This kinetic nature of the lattice Boltzmann method provides some superior features, such as the linearity of the transport equation (in comparison with nonlinear Navier-Stokes equations), and calculation of pressure by an equation of state (in comparison with calculating the pressure by solving Poisson differential equation) [13].

The present numerical model is based on the lattice Boltzmann method with a single relaxation time collision operator (the so-called BGK model [24]) and the popular D2Q9 lattice scheme. The "2" in D2Q9 refers to the number of lattice dimensions and the "9" denotes the number of possible directions for a particle movement in the lattice.

The lattice Boltzmann equation is derived from the simplification of Boltzmann equation in a lattice [25]. It can be expressed as

$$f_i(\vec{r}+\vec{c}_i\Delta t,\, t+\Delta t) = f_i(\vec{r},\, t) + \frac{\Delta t}{\tau_f}\left[f_i^{eq}(\vec{r},\, t) - f_i(\vec{r},\, t)\right] \tag{1}$$

where f_i is the density distribution function in direction i, f_i^{eq} is the equilibrium density distribution function, $\vec{r}$ refers to space position, t is time, $\vec{c}$ is the velocity vector in direction i, and τ_f is the fluid flow relaxation time which is related to kinematic viscosity, ν, by $\tau_f = 3\nu + 1/2$. The equilibrium density distribution function is determined by

$$f_i^{eq} = w_i\rho\left[1 + \frac{\vec{c}_i\cdot\vec{u}}{c_s^2} + \frac{1}{2}\frac{(\vec{c}_i\cdot\vec{u})^2}{c_s^4} - \frac{1}{2}\frac{\vec{u}\cdot\vec{u}}{c_s^2}\right] \tag{2}$$

In this equation, w_i is the weighting factor, $\rho = \sum_i f_i$ is the fluid density, $\vec{u} = \sum_i f_i\vec{c}_i / \sum_i f_i$ is fluid velocity and c_s is the speed of sound in the lattice.

Eq. (1) is solved through collision and streaming processes, which are shown for D2Q9 scheme in Eqs. (3) and (4), respectively.

$$f_i(x, y, t+\Delta t) = f_1(x, y, t)\left[1 - \frac{\Delta t}{\tau_f}\right] + \frac{\Delta t}{\tau_f}f_i^{eq}(x, y, t) \tag{3}$$

$$f_i(x+\Delta x, y+\Delta y, t+\Delta t) = f_i(x, y, t+\Delta t) \tag{4}$$

To completely determine density distribution functions, f_is must be specified at the boundaries. A simple and powerful LBM boundary condition applied to no-slip walls is called the "bounce back" boundary condition. This boundary condition is based on the idea that particles colliding a wall in a direction will bounce back in the opposite direction [26]. In fact, this boundary condition enables LBM to model fluid flow in geometries with complicated microstructure, such as pore space of a porous medium. Several versions of this boundary condition have been proposed [22]; however, the most-used version is the half-way method in which the wall is located half-way between two neighboring grids.

The remaining part of this section will look at the important aspects of the numerical method applied for simulation of ammonia cracking microreactor. More specifically, to propose a numerical method for simulation of velocity and concentration field, the simulation of multi-species gas flow consisting of ammonia, hydrogen and nitrogen is described at first. Next, the method of simulating surface reaction is presented, and finally, the method of simulating temperature field will be explained.

2. Simulation of Multi-species Flow

Generally, two passive and active approaches are used for simulating multi-species gas flow (single-phase multi-component flow in LB terminology). In the passive approach, the chemical species whose mass fraction is greater than the others is considered as solvent while other species are considered as solutes. In this way, the velocity field is only solved for the solvent species, followed by the solution of advection-diffusion concentration equation for the other species. Therefore, the velocity field is only dependent on the solvent species. However, when the solvent species concentration is not dominant, this may lead to the lack of accuracy [22].

On the other hand, the internally coupled velocity fields of all species are solved individually in the active approach; hence, more accurate results can be obtained by the more realistic active approach. To utilize this approach in lattice Boltzmann method, multi-phase multi-component models are adopted and some of their settings are tuned to reduce the number of phases to one.

Several multi-phase multi-component LB models have been presented in the literature [27-29]. In the present study, the Shan and Chen model [28] is selected for its simplicity and ease of implementation. The number of phases in this method is reduced to one by only eliminating the inter-particle forces [22]. Therefore, to implement the Shan and Chen model for single-phase flow consisting of ammonia, hydrogen and nitrogen species, the streaming and collision processes are solved individually for each species to find f_i^k, where the superscript k denotes the *k*th chemical species. However, in the collision process the composite velocity, $\vec{u}'$, must be incorporated instead of $\vec{u}^k$ in Eq. (2) to couple the lattice Boltzmann equations of different species. The composite velocity is defined as

$$\vec{u}' = \frac{\sum_k \frac{1}{\tau_f^k} \sum_i f_i^k \vec{c}_i}{\sum_k \frac{1}{\tau_f^k} \rho^k} \tag{5}$$

In the above equation, τ_f^k and $\rho^k = \sum_i f_i^k$ are the relaxation time and the density of kth species, respectively. τ_f^k is related to the kinematic viscosity of kth species, ν^k, by the relation $\tau^k = 3\nu^k + 1/2$.

3. Simulation of Surface Reaction

Generally, chemical reactions are either exothermic (generating heat) or endothermic (absorbing heat). The endothermic chemical surface reaction occurring in an ammonia cracking microreactor can be expressed as:

$$NH_3 \rightarrow \frac{1}{2}N_2 + \frac{3}{2}H_2 \tag{6}$$

Using Ni-Pt/Al_2O_3 as the catalyst, Chellappa et al. [30] performed experimental studies and suggested that when the operating pressure is around 1 atm, the reaction is first order on the NH_3 concentration as follows:

$$r = 1.309 \times 10^{12} \exp\left(-\frac{49229}{RT}\right) p_{NH_3} \tag{7}$$

where ammonia partial pressure (p_{NH_3}) and RT must be used in bar and cal mol^{-1}, respectively; the resulting rate will be in mol gCa^{-1} h^{-1}. By applying catalyst surface-to-volume ratio, catalyst density, ideal gas relation and also some unit conversions, the above equation can be converted to the following one:

$$r'' = 1.158 \times 10^{14} \exp\left(-\frac{24774}{T}\right) \frac{\rho_{NH_3}}{T} \tag{8}$$

where temperature (T), ammonia density (ρ_{NH_3}) and surface reaction rate (r″) are in K, mol m^{-3} and mol m^{-2} s^{-1}, respectively. If the temperature at a lattice surface node is known, the above equation can be simplified as $r'' = k_{sr}\rho_{NH_3}$ in which:

$$k_{sr} = \frac{1.158 \times 10^{14}}{T} \exp\left(-\frac{24774}{T}\right) \tag{9}$$

After determining k_{sr} for the reactive surface nodes of a lattice, the proposed method by Kamali et al. [31] for the first-order surface reactions can be adopted to simulate the surface reaction of ammonia decomposition. The main idea of the proposed method is based on the modifying of the bounce-back boundary condition (mentioned in Section 2.1). In this regard, when an NH_3 particle collides with a reactive surface, its mass decreases by a factor of $1-k_{sr}^{LB}$ where k_{sr}^{LB} ($0<k_{sr}^{LB}<1$) can be calculated as:

$$k_{sr}^{LB} = \left(\frac{6k_{sr}\Delta t}{\Delta x}\right) / \left(1 + \frac{k_{sr}\Delta x}{2D}\right) \tag{10}$$

where k_{sr} is the rate constant of surface reaction (calculated by Eq. (9)), Δt and Δx are the time interval and space interval in direction normal to the surface, and D is the diffusion coefficient of NH_3. Subsequently, the mass of a hydrogen particle and a nitrogen particle colliding with a reactive surface will be increase as a factor of $(1+(3/2)(MW_{H_2}/MW_{NH_3})k_{sr}^{LB})$ and $(1+(1/2)(MW_{N_2}/MW_{NH_3})k_{sr}^{LB})$, respectively; where MW_{NH_3}, MW_{H_2} and MW_{N_2} indicate molar mass of ammonia, hydrogen and nitrogen, respectively. The complete derivation of the proposed method accompanied by its validation can be found in the previous studies [32,33]. Note that although only NH_3 decomposition is simulated in the present study, the presented numerical model is general and can be used for other kinds of first-order surface reactions in a porous medium with complicated microstructure.

4. Simulation of Conjugate Heat Transfer

The computational domain for simulation of a microreactor consists of void regions and solid regions. In the void regions, the heat is transferred via the convection mechanism, while in the solid regions the heat transfer mechanism is conduction. The temperature and the heat flux at the interfaces of these two regions are not known, so we are faced with a conjugate heat transfer problem. The fact that due to the endothermic surface reaction a heat sink is located at the interface of a void region and a solid region makes the situation more complicated. However, contrasting its complicated physics, it can be simply treated by LBM as presented and well-established in the literature [25]. To do so, adopting D2Q4 LB scheme, the following lattice Boltzmann equation must be solved:

$$g_i(\vec{r} + \vec{c}_i\Delta t, t + \Delta t) = g_i(\vec{r}, t) + \frac{\Delta t}{\tau_g}[g_i^{eq}(\vec{r}, t) - g_i(\vec{r}, t)] + w_i S^{LB}\Delta t \tag{11}$$

where g_i is the thermal density distribution function in direction i, g_i^{eq} is the equilibrium density distribution function, τ_g is the heat transfer relaxation time, which is related to thermal diffusion coefficient (α) by $\tau_g = 3\alpha + (1/2)$ and S^{LB} is heat sink power, which is a function of reaction rate expression. The thermal equilibrium density distribution functions of Eq. (11) can be evaluated more simply than the fluid flow equilibrium density distribution functions of Eq. (2) as follows:

$$g_i^{eq} = w_i T\left[1 + \frac{\vec{c}_i \cdot \vec{u}}{c_s^2}\right] \text{ for void regions} \tag{12}$$

$$g_i^{eq} = w_i T[1] \text{ for solid regions}$$

where c_s is the sound velocity ($1/\sqrt{2}$ for the D2Q4 Scheme) and $t = \sum_i g_i$ is the gas or solid phase temperature. After calculating g_i^{eq} for each nodes of the lattice, the density distribution functions can be evaluated through collision and streaming processes as presented in Eqs. (3) and (4).

5. Model Validation

As mentioned, the kinetic nature of the presented model has been validated in the previous works [32,33]. However, the presented model is also validated via experimental results of Chellappa et al. [30]. They measured ammonia conversion in a microreactor with catalyst particles of 40 μm in various temperatures. To mitigate the departure of our 2D model from the real 3D microreactor, a post microreactor with 26.7 μm diameter cylindrical posts is simulated, which has the same surface to mass ratio as the Chellappa et al. microreactor. Shown in Table 1 is a comparison of simulation results with Chellappa et al. experimental results for four different temperatures: 560 °C, 580 °C, 620 °C and 660 °C. The inlet ammonia flow rates for these four different simulations were selected such that the catalyst loading to ammonia flow rate of each simu-

Table 1. Comparison of simulation results with Chellappa et al. [30] measurements

Temperature	Ammonia conversion (simulation)	Ammonia conversion (measurement)
560 °C	0.9445	0.916
580 °C	0.9212	0.876
620 °C	0.9398	0.898
660 °C	0.9523	0.906

lation would be the same as that of Chellappa et al. [30]. The relative difference of simulation results with experimental data does not exceed 6%. However, we believe that if more detailed information about the microreactor microstructure were available, the relative difference would be much less than 6%.

COMPUTATIONAL DOMAIN AND BOUNDARY CONDITIONS

In the current investigation, five different microreactors with different microstructures and the same amount of catalyst are simulated and analyzed. The catalyst is embedded in a channel which is 480 μm wide and 2,500 μm long (Fig. 1). A 500 μm length of the entering region and also the exiting region of the channel is considered catalyst-free. The height of the channel is considered to be the same as its width. Two of the simulated microreactors are post microreactors, one with square shaped posts and the other with circle shaped posts. The posts have a 5×15 in-line arrangement in which the centers of the posts are 100 μm far from each other. The length of a square post is 50 μm and the diameter of a circle post is 56 μm. Three simulated microreactors are microfibrous ones in which the catalyst is composed of thin fibers with 8 μm diameter, the same as the nickel fibers diameter reported in the literature [3,34]. The first microfibrous microreactor has fibers which are all aligned horizontally, just such as an ideal case (Fig. 2(a)). However, the catalytic fibers in a microreactor have dissimilar orientations. Hence, in the second microfibrous microreactor, some parts of the horizontal fibers are aligned upward right (Fig. 2(b)); and finally, in the third microfibrous microreactor, some parts of the horizontal fibers are aligned upward right and some parts are aligned upward left, which seems such as an isotropic situation (Fig. 2(c)). Although these three microstructures are not realistic representations of microfibrous media, they have been chosen to explore the impact of the fiber orientation.

Pure ammonia with uniform pressure and temperature (1.0 atm and 560 °C) enters from the inlet, and after cracking into hydrogen and nitrogen exits with 1.1 atm total pressure from the outlet. Each mole of ammonia cracks to 2 moles of products (1.5 mole H_2 and 0.5 mole N_2), and hence the increase of pressure is inevitable. In fact, a very fast reaction with no frictional pressure loss can make the outlet pressure twice of the inlet pressure. The temperature gradient at the outlet is considered to be zero. To implement inlet and outlet pressure boundary conditions, the Zou and He method [35] is utilized. Since only the total outlet pressure is known and the outlet partial pressure of each species is unknown, these partial pressures are determined by assuming that the mole fraction of each species at the outlet is equal to that at the preceding nodes; this is a reasonable assumption since species fraction will not change much through a lattice unit near the outlet region (1 μm). Upon determining outlet partial pressure of each species, constant pressure boundary condition of Zou and He [35] is applied for each species.

The channel walls are considered as the no-slip constant temperature (560 °C) surfaces. Based on the proposed model, a parallel FORTRAN code based on Open MP is developed and implemented on a core i7 home-based computer for the simulations. The developed code has six main subroutines for considering col-

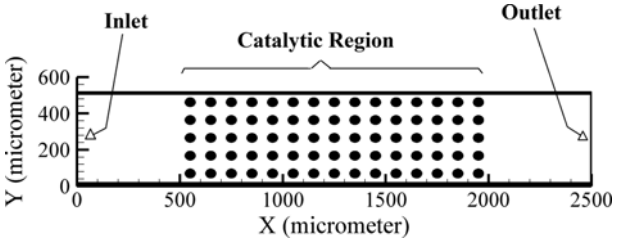

Fig. 1. Computational domain: The microstructure of catalytic region differs in the simulated microreactors.

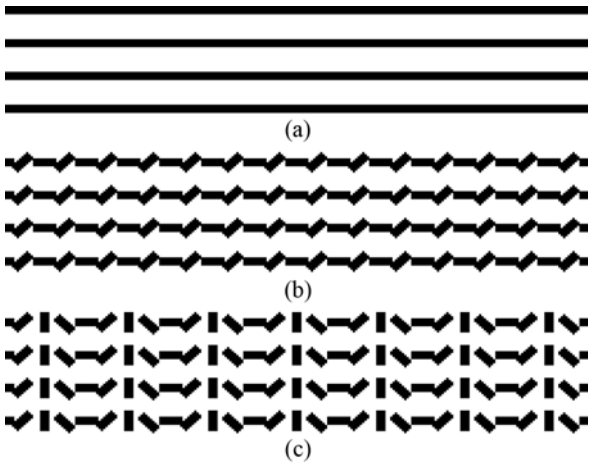

Fig. 2. Microstructure of simulated microfibrous microreactors: (a) First microfibrous microreactor, (b) second microfibrous microreactor, (c) third microfibrous microreactor.

Table 2. The value of simulation parameters

Parameter	Value
Microreactor length	2500 μm
Microreactor width	480 μm
Length of catalytic region	1500 μm
Inlet pressure	1.0 atm
Pressure differential between inlet and outlet	0.1 atm
Initial partial pressure of ammonia	1.0 atm
Initial partial pressure of hydrogen	0.0 atm
Initial partial pressure of nitrogen	0.0 atm
Initial temperature	560 °C
Inlet flow temperature	597 °C
Outer surface temperature	560 °C

lision, streaming and boundary conditions of the flow and heat density distribution functions. Each unit of the generated lattice is 2 μm long. Also, a time step duration is 2.380952×10^{-8} s. The values of simulation parameters are presented in Table 2.

RESULTS AND DISCUSSION

The ammonia partial pressure distribution for all five simulated microreactors is presented in Fig. 3. The ammonia partial pressure decreases by crossing the microreactor length from left to right and cracking on the surfaces of posts or fibers. Figs. 3(a) and (b) show that when a post microreactor is applied, the partial pressure of ammonia decreases to about 0.5 atm, which is far from an ideal microreactor in which the partial pressure at the outlet reaches zero. As shown in Fig. 3(c), when all parts of the fibers are aligned horizontally (first microfibrous microreactor) the ammonia partial

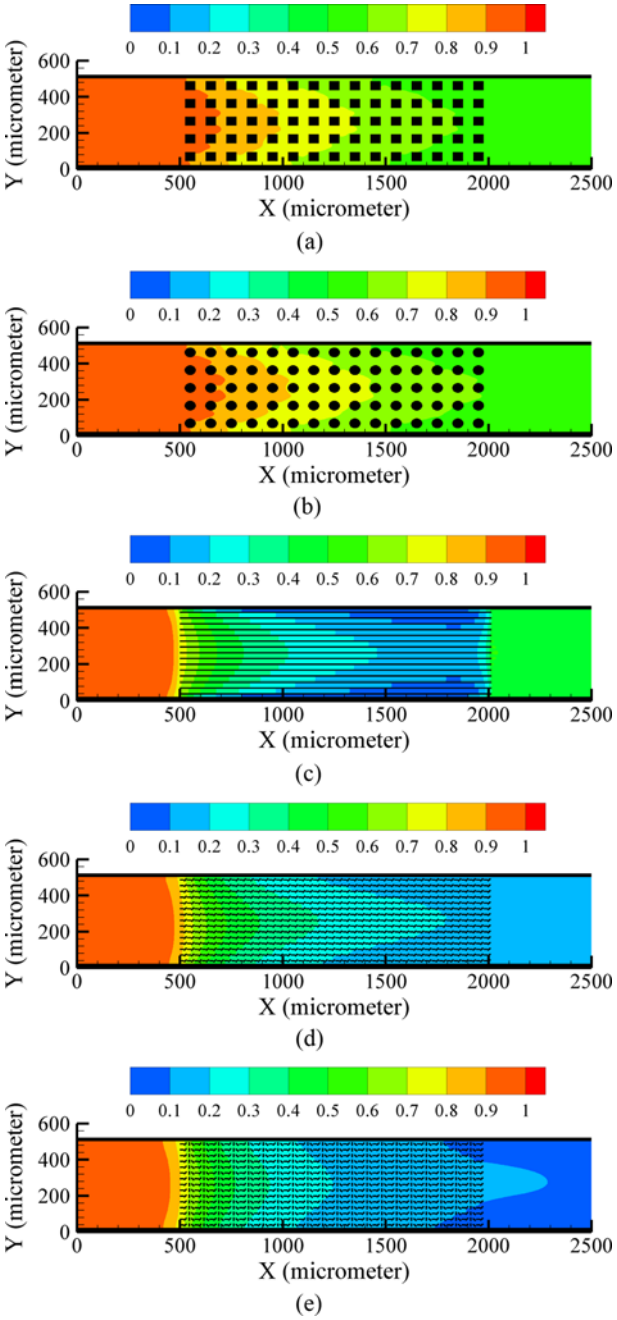

Fig. 3. Ammonia partial pressure distributions (atm) for the five simulated microreactors: (a) Square post microreactor, (b) circle post microreactor, (c) first microfibrous microreactor, (d) second microfibrous microreactor, (e) third microfibrous microreactor.

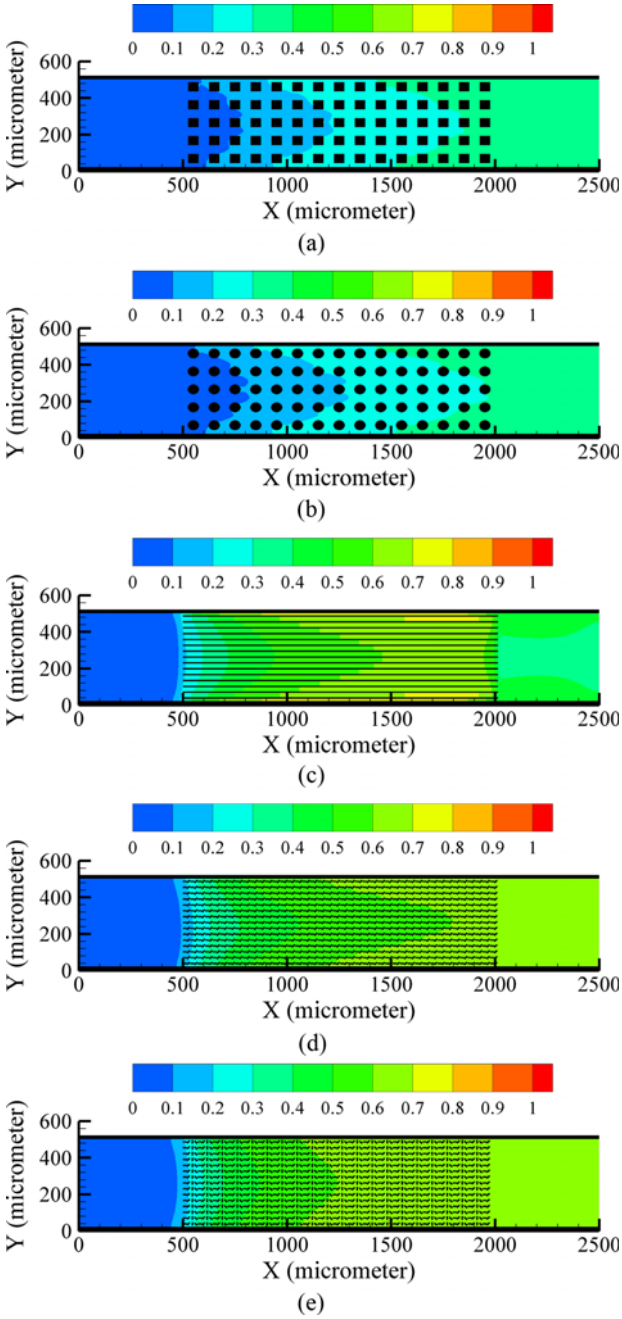

Fig. 4. Hydrogen partial pressure distributions (atm) for the five simulated microreactors: (a) Square post microreactor, (b) circle post microreactor, (c) first microfibrous microreactor, (d) second microfibrous microreactor, (e) third microfibrous microreactor.

pressure at the outlet is about 0.4 atm, which indicates an insufficient ammonia conversion of this microreactor as well. However, as shown in Figs. 3(d) and (e), in the second and third microfibrous microreactors, in which some parts of fibers are aligned non-horizontally, ammonia partial pressure reaches 0.1 atm at the outlet, which shows the superiority of these two microfibrous microreactors. This superiority is not only due to the microfibrous microstructure, but also the fiber orientation. It demonstrates the fact that when all parts of the fibers are aligned horizontally, the ammonia cracking will not be efficient. This inefficiency stems from thermal reasons which will be discussed later.

The partial pressure of hydrogen and nitrogen for all five microreactors is presented in Figs. 4 and 5, respectively. Comparison of Figs 4(a)-(e) shows that the outlet partial pressure of the hydrogen in the second and third microfibrous microreactors is much higher than the first microfibrous microreactor, and the partial pressure of the outlet hydrogen in the first microfibrous microreactor is higher than the post microreactors, which illustrates the dissimilar

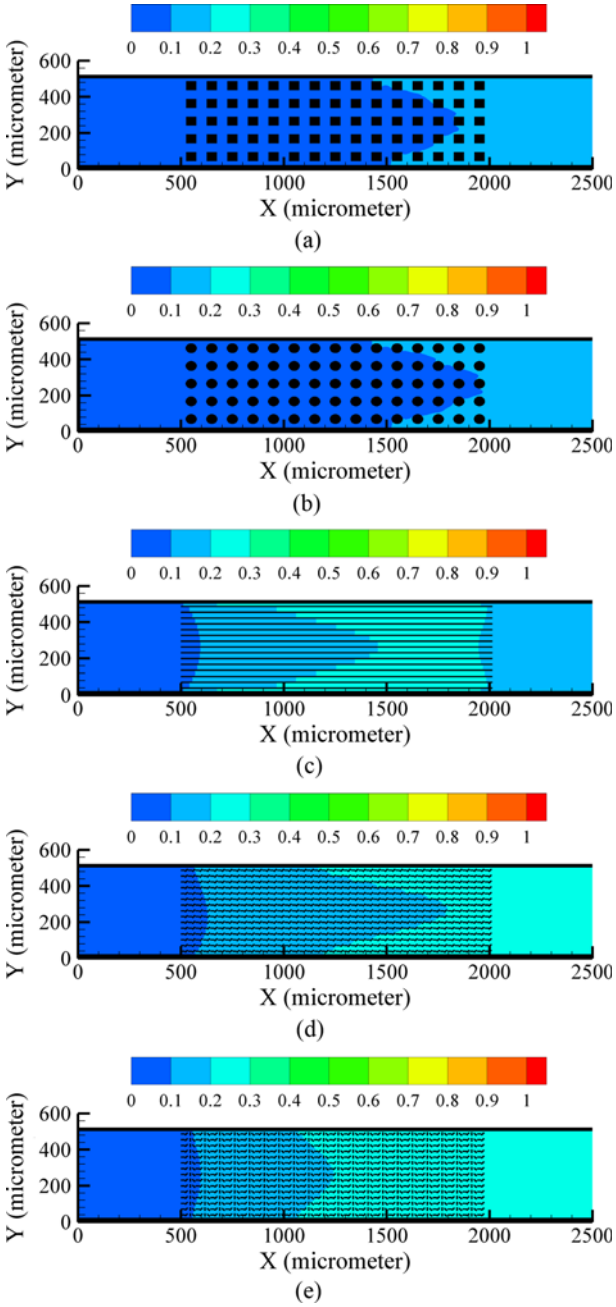

Fig. 5. Nitrogen partial pressure distributions (atm) for the five simulated microreactors: (a) Square post microreactor, (b) circle post microreactor, (c) first microfibrous microreactor, (d) second microfibrous microreactor, (e) third microfibrous microreactor.

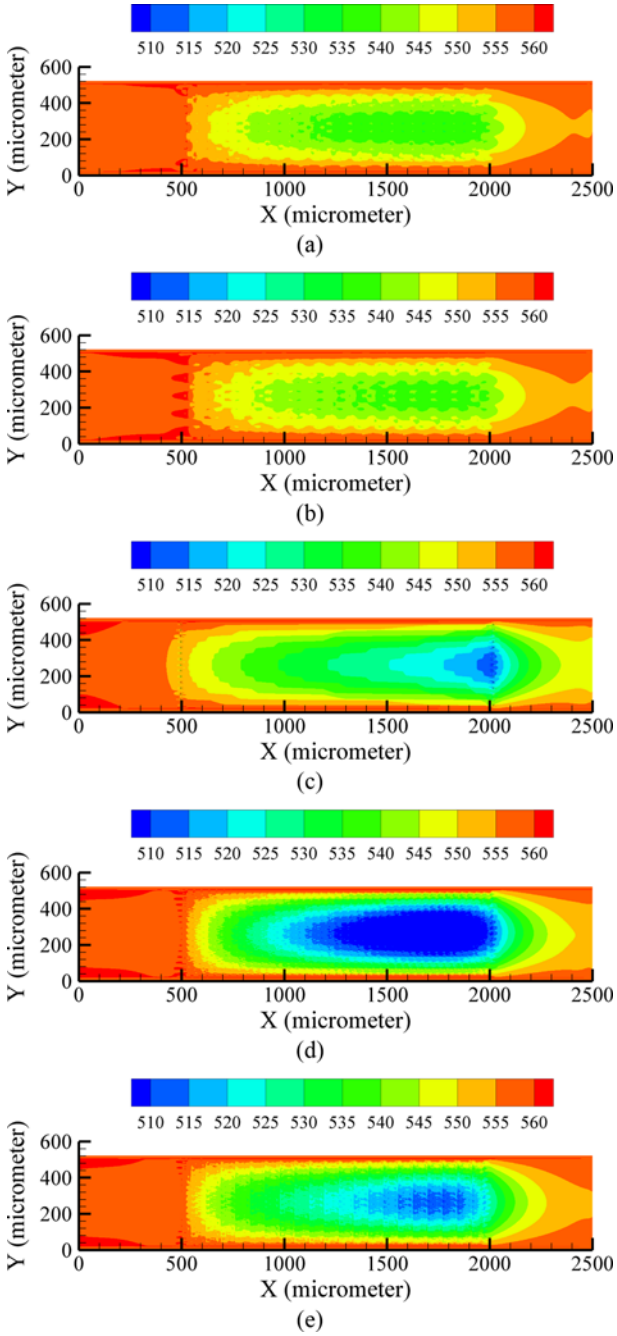

Fig. 6. Temperature distributions (°C) for the five simulated microreactors: (a) Square post microreactor, (b) circle post microreactor, (c) first microfibrous microreactor, (d) second microfibrous microreactor, (e) third microfibrous microreactor.

ammonia cracking efficiencies of the simulated microreactors.

Figs 4(a)-(e) also show that hydrogen partial pressure is higher near microreactor walls rather than near its centerline; this is a result of higher temperature of the walls relative to the interior zone. In fact, the temperature of microreactor walls equals 560 °C, while the interior temperature is less due to endothermic nature of ammonia cracking reaction occurring in the interior zone. A similar manner can be seen for the partial pressure of nitrogen in Figs. 5(a)-(e).

A rough comparison of Figs. 4 and 5 shows that the hydrogen partial pressure is about three times of the nitrogen partial pressure (each mole of ammonia cracks into 1.5 mole of hydrogen and 0.5 mole of nitrogen). However, the ratio does not exactly equal three at all locations; this is because hydrogen and nitrogen have different viscosities. The effect of dissimilar viscosities of species on their concentration distribution can only be captured by an active approach.

Shown in Fig. 6 is the temperature distribution for all five simulated microreactors. The temperature field has a cold core surrounded by a warm region. The cold core is approximately adjusted the catalytic region in which the chemical reaction occurs. Comparison of Figs. 6(a)-(e) shows that the cold core has a lower temperature in the second and third microfibrous microreactors relative to the first microfibrous microreactor, and the cold core has a lower temperature in the first microfibrous microreactor relative to the post microreactors. This fact indicates that more ammonia conversion, and subsequently more heat consumption, occurs in the second and third microfibrous microreactors; thus, they are more efficient microreactors.

Fig. 7 illustrates the time evolution of ammonia conversion for all five simulated microreactors. Ammonia conversion, which is the ratio of converted quantity of ammonia to its inlet quantity, is a scale to evaluate the hydrogen production efficiency of a microreactor. In all cases, the ammonia conversion has an oscillating manner versus time duration; however, the steady state condition is attained after about 600,000 time steps which equals 14.286 ms. The steady state ammonia conversion in the third microfibrous microreactor is a bit greater that the second one, which may be due to the fact that in the third microfibrous microreactor further parts of fibers are aligned non-horizontally. The ammonia conversion of the first microfibrous microreactor is less than the other two microfibrous microreactors; however, it is greater than the ammonia conversion of the post microreactors; this is by the reason of its larger reactive surface. Fig. 7 also indicates that the post shape (circle or square) does not have a significant effect on the ammonia conversion.

Figs. 8(a) and (b) show the time evolution of average heat flux on the upper and lower walls of all simulated microreactors, respectively. The third and the second microfibrous microreactors experience a larger heat flux, which is because ammonia conversion in these two microreactors is greater than the others, and as a result more thermal energy is needed, which leads to a larger heat flux through microreactor walls. Figs. 8(a) and (b) also show that the average heat fluxes in the first microfibrous microreactor and the two post microreactors are almost the same.

Presented in Fig. 9 is the time evolution of ammonia flow rate through the inlet of simulated microreactors. Similar to the heat flux, the steady state ammonia flow rate in the first microfibrous

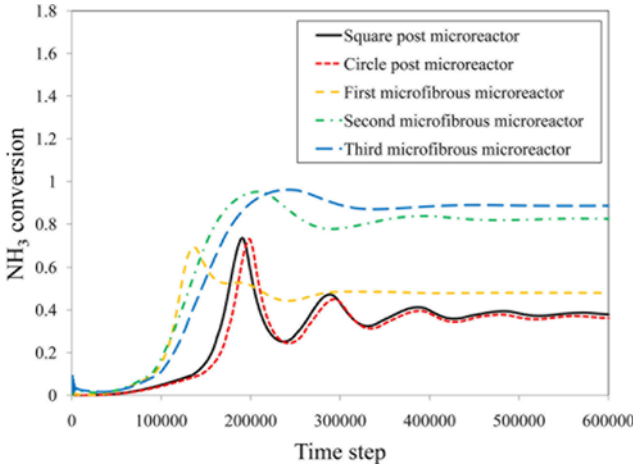

Fig. 7. The time evolution of ammonia conversion for the five simulated microreactors.

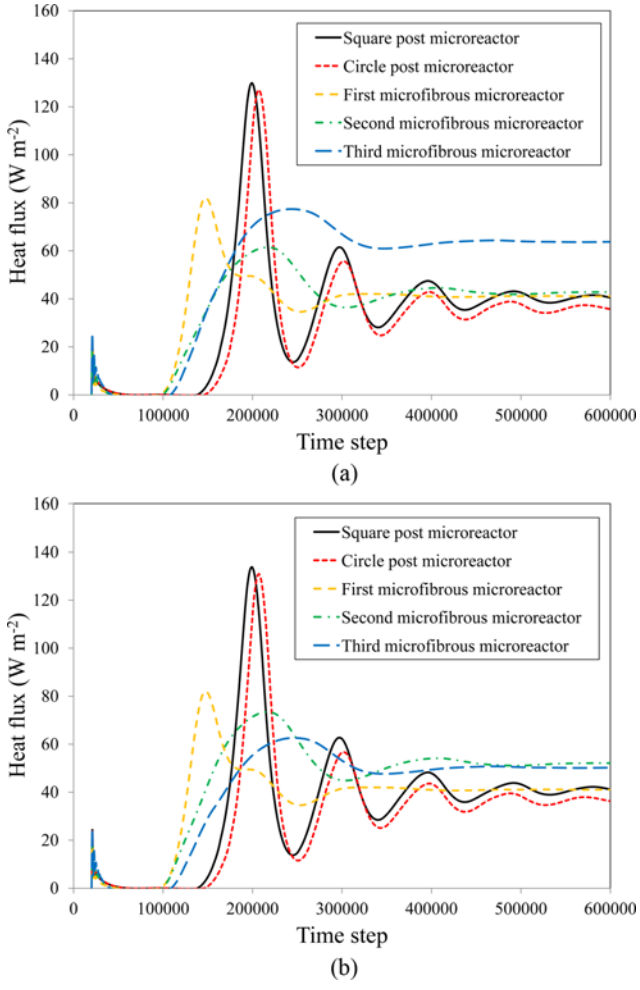

Fig. 8. The time evolution of average heat flux (W m^{-2}) for the five simulated microreactors: (a) On the upper wall of microreactors, (b) on the lower wall of microreactors.

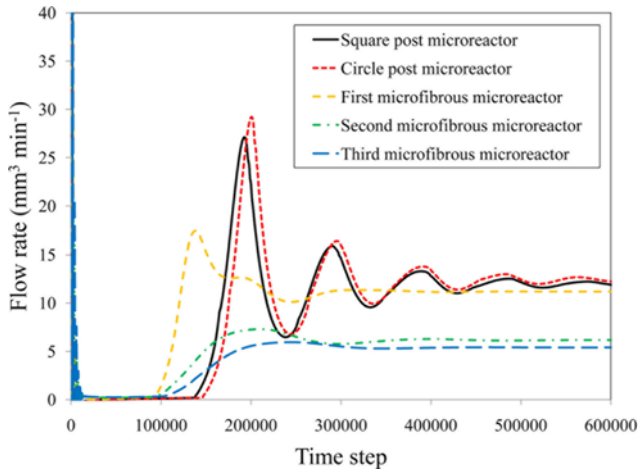

Fig. 9. The time evolution of ammonia flow rate ($mm^2\ min^{-1}$) for the five simulated microreactors.

microreactor is almost the same as in the two post microreactors. The ammonia flow rate in the second and third microfibrous microreactors is lower than the other microreactors for a constant pressure differential between the inlet and the outlet; i.e. for a constant flow rate, the second and third microfibrous microreactors experience a larger pressure drop which reveals that more friction appears in these two microreactors.

Figs. 7-9 demonstrate the fact that ammonia conversion for a microfibrous microreactor with more not-horizontally aligned fiber parts is superior; however, the heat flux and the flow rate are inferior. The role of fiber orientation on the performance of microfibrous microreactors can be further investigated by 3D simulations performed based on the LB model presented in this study.

CONCLUSIONS

A numerical model based on the lattice-Boltzmann method (LBM) is presented to investigate ammonia cracking microreactors with coupled physiochemical thermal processes at the pore-scale. Several sets of transport phenomena such as fluid flow, species transport, heat transfer and chemical reaction are taken into account in this model. Moreover, to model the species transport an active approach is applied which has a higher accuracy relative to common passive approaches. Three microfibrous microreactors and two post microreactors are simulated by the presented numerical model. Post microreactors display the worst performance. Among the microfibrous microreactors, the one which has more fiber parts aligned non-horizontally has the best ammonia conversion efficiency. However, its flow rate and heat consumption are the worst. The results of this study confirm the important role of fibers orientation on the performance of a microfibrous microreactor.

NOMENCLATURE

$\vec{c}_i$: particle velocity in direction i of lattice [lu ts^{-1*}]
c_s : speed of sound in lattice [lu ts^{-1}]
D : ammonia diffusivity [$m^2\ s^{-1}$]
D^{LB} : ammonia Lattice Boltzmann diffusivity [$lu^2\ s^{-1}$]
f : density distribution function for fluid flow
g : density distribution function for heat transfer
k_{sr} : rate constant of surface reaction [m s^{-1}]
k_{sr}^{LB} : Lattice-Boltzmann rate constant of surface reaction
MW : nolar mass [kg $kmol^{-1}$]
p : partial pressure [Pa]
R_u : universal gas constant [J $mol^{-1}\ K^{-1}$]
$\vec{r}$: particle position vector [lu]
r : rate of reaction based on per unit mass of catalyst [mol $gCa^{-1}\ h^{-1}$]
r″ : rate of reaction based on per unit surface of catalyst [mol $m^{-2}\ s^{-1}$]
S^{LB} : Lattice-Boltzmann sink of heat transfer
T : temperature [K]
t : time [ts]
$\vec{u}$: velocity vector [lu ts^{-1}]
$\vec{u}'$: composite velocity vector in Eq. (5) [lu ts^{-1}]
w : weighting factor

Greek Symbols

α : thermal diffusivity [$m^2\ s^{-1}$]
ν : kinematic viscosity [$lu^2\ ts^{-1}$]
ρ : density [lm lu^{-3} or kg m^{-3}]
τ_f : relaxation time for fluid flow [ts]
τ_g : relaxation time for heat transfer [ts]

Subscripts and Superscripts

eq : equilbrium
i : direction i of lattice
k : *k*th Species
LB : Lattice-Boltzmann
ref : refrence
sr : surface reaction

REFERENCES

1. M. Ehsani, Y. Gao, S. E. Gay and A. Emadi, *Modern electric, hybrid electric and fuel cell vehicels*, CRC Press, London (2012).
2. J. Larminie and A. Dicks, *Fuel cell systems explained*, Wiley, Chichester (2003).
3. M. Wang, J. Li, L. Chen and Y. Lu, *Int. J. Hydrogen Energy*, **34**, 1710 (2009).
4. O. Worz, K. P. Jackel, T. Richter and A. Wolf, *Chem. Eng. Technol.*, **24**, 138 (2001).
5. K. F. Jensen, *Chem. Eng. Sci.*, **56**, 293 (2001).
6. G. Kolb and V. Hessel, *Chem. Eng. J.*, **98**, 1 (2004).
7. M. Karakaya, S. Keskin and A. K. Avci, *Appl. Catal. A*, **411**, 114 (2012).
8. J. J. Lerou, M. P. Harold, J. Ryley, J. Ashmead, T. C. O'Brien, M. Johnson, J. Perrotto, C. T. Blaisddell, T. A. Rensi and J. Nyquist, in *Microsystem technology for chemical and biological microreactors*, W. Ehrfield Eds., DECHEMA, New York (1996).
9. S. Chiuta, R. C. Everson, H. W. J. P. Neomagus, P. Van der Gryp

* lu and ts are the unit of length and time in lattice Boltzmann method, respectively.

and D. G. Bessarabov, *Int. J. Hydrogen Energy*, **38**, 14968 (2013).
10. M. S. Shin, N. Park, M. J. Park, K. W. Jun and K. S. Ha, *Chem. Eng. J.*, **234**, 23 (2013).
11. M. S. Shin, N. Park, M. J. Park, J. Y. Cheon, J. K. Kanga, K. W. Jun and K. S. Ha, *Fuel Process. Technol.*, **118**, 235 (2014).
12. D. Y. Shin, K. S. Ha, M. J. Park, G. Kwak, Y. J. Lee and K. W. Jun, *Fuel*, **158**, 826 (2015).
13. S. Chen and G. D. Doolen, *Annu. Rev. Fluid Mech.*, **30**, 329 (1998).
14. T. Zeiser, P. Lammers, E. Klemm, Y. W. Li, J. Bernsdorf and G. Brenner, *Chem. Eng. Sci.*, **56**, 1697 (2001).
15. H. Freund, T. Zeiser, F. Huber, E. Klemm, G. Brenner, F. Durst and G. Emig, *Chem. Eng. Sci.*, **58**, 903 (2003).
16. M. Nijemeisland and A. G. Dixon, *AIChE J.*, **50**, 906 (2004).
17. S. P. Sullivan, F. M. Sani, M. L. Johns and L. F. Gladden, *Chem. Eng. Sci.*, **60**, 3405 (2005).
18. N. Manjhi, N. Verma, K. Salem and D. Mewes, *Chem. Eng. Sci.*, **61**, 2510 (2006).
19. P. H. Kao, T. F. Ren and R. J. Yang, *Int. J. Heat Mass Transfer*, **50**, 4243 (2007).
20. N. Verma, K. Salem and D. Mewes, *Chem. Eng. Sci.*, **62**, 3685 (2007).
21. L. Chen, Q. Kang, Y. L. He and W. Q. Tao, *Int. J. Hydrogen Energy*, **37**, 13943 (2012).
22. M. C. Sukop and D. T. Thorne, *Lattice Boltzmann Modeling, An Introduction for Geoscientists and Engineers*, Springer, Heidelberg (2007).
23. A. Satoh, *Introduction to practice of molecular simulation*, Elsevier Inc., Amsterdam (2011).
24. P. L. Bhatnagar, E. P. Gross and M. Krook, *Phys. Rev.*, **94**, 511 (1954).
25. A. A. Mohamad, *Lattice Boltzmann Method-Fundamentals and Engineering Applications with Computer Codes*, Springer, Heidelberg (2011).
26. S. Succi, *The Lattice Boltzmann Equation for Fluid Dynamics and Beyond Numerical Mathematics And Scientific Computation*, Clarendon Press, Oxford (2001).
27. A. K. Gunstensen, D. H. Rothman, S. Zaleski and G. Zanetti, *Phys. Rev. A*, **43**, 4320 (1991).
28. X. Shan and H. Chen, *Phys. Rev. E*, **47**, 1815 (1993).
29. M. R. Swift, W. R. Osborn and J. M. Yeomans, *Phys. Rev. Lett.*, **75**, 830 (1995).
30. A. S. Chellappa, C. M. Fischer and W. J. Thomson, *Appl. Catal. A*, **227**, 231 (2002).
31. M. R. Kamali, S. Sundaresan, H. E. A. Van den Akker and J. J. J. Gillissen, *Chem. Eng. J.*, **207-208**, 587 (2012).
32. G. R. Molaeimanesh and M. H. Akbari, *J. Power Sources*, **258**, 89 (2014).
33. G. R. Molaeimanesh and M. H. Akbari, *Korean J. Chem. Eng.*, **32**, 397 (2015).
34. Y. Liu, H. Wang, J. Li, Y. Lu, H. Wu, Q. Xue and L. Chen, *Appl. Catal. A*, **328**, 77 (2007).
35. Q. Zou and X. He, *Phys. Fluids*, **9**, 1591 (1997).